Chinese Chemical Letters 34 (2023) 108100

Contents lists available at ScienceDirect

Chinese Chemical Letters

journal homepage: www.elsevier.com/locate/cclet

A chiral $SrSi_2$ (srs) superstructure constructed by a dual interaction system showing isotropic electrical conductivity

Jin Liu[a,b,c], Zi-Xiu Lu[a,c], Fa-Fa Wu[d], Guo-Ling Li[a,c], Bin Wang[a,c], Xue-Li Cao[a,c], Wei Wang[a,c], Zhu Zhuo[a,c], Qiao-Hong Li[d,*], You-Gui Huang[a,c,e,*]

[a] CAS Key Laboratory of Design and Assembly of Functional Nanostructures, and Fujian Provincial Key Laboratory of Nanomaterials, Fujian Institute of Research on the Structure of Matter, Chinese Academy of Sciences, Fuzhou 350002, China
[b] University of Chinese Academy of Sciences, Beijing 100049, China
[c] Xiamen Key Laboratory of Rare Earth Photoelectric Functional Materials, Xiamen Institute of Rare Earth Materials, Haixi Institutes, Chinese Academy of Sciences, Xiamen 361021, China
[d] State Key Laboratory of Structure Chemistry, Fujian Institute of Research on the Structure of Matter, Chinese Academy of Sciences, Fuzhou 350002, China
[e] Fujian Science & Technology Innovation Laboratory for Optoelectronic Information of China, Fuzhou 350108, China

ARTICLE INFO

Article history:
Received 7 November 2022
Revised 4 December 2022
Accepted 22 December 2022
Available online 24 December 2022

Keywords:
Electrical conductivity
Self-assembly
Isotropic
$\pi\cdots\pi$ Interactions
Chiral

ABSTRACT

Most porous conductive frameworks are highly anisotropic in their structures thus leading to anisotropic charge transport. Here we report a supramolecular self-assembly which is constructed by intermolecular hydrogen bonding and $\pi\cdots\pi$ interactions. This material features a chiral, porous, cubic framework structure with π-stacked helical columns along all of the three Cartesian coordinates. As a result, isotropic charge transport with an electrical conductivity (σ) of 2.1×10^{-7} S/cm is achieved. By achieving isotropic charge transport in a π-stacked supramolecular assembly, these results provide a new type of isotropic conductive framework materials alternative to conductive metal-organic frameworks (MOFs).

Recent emergence and advances in electrically conductive porous frameworks have brought a variety of important applications, such as chemiresistive sensing [1–4], electrochemical energy storage [5,6,7,8,9], and electrocatalysis [10–12]. The vast majority of these conductive framework structures are metal-organic frameworks (MOFs), and highly conductive MOFs have been achieved for the great efforts paid on enhancing charge mobility in MOFs [13,14]. For example, the conductivities of MOFs constructed by ligands with catechol- or semiquinone-derived groups can reach as high as $\sim 10^{-1}$ S/cm [15–18]. Yet most MOFs are anisotropic [1,19,20], charge transport pathways in these anisotropic materials are a 1D metal–ligand chain [21–23], a $\pi\cdots\pi$ stacked column [24–28], or a π-conjugated sheet [29–31]. Although low-dimensional charge transport is very desired in certain circumstances, it is also important to design conductive frameworks with isotropic charge transport. Herein, isotropic charge transport is defined as direction-independent electrical conductivity. Typically, the charge transport in a single crystal with a cubic structure is direction-independent, thus a cubic structure shows isotropic electrical conductivity. However, as best as we known only very limited frameworks exhibit isotropic charge transport. Representative examples include several metal-triazolates and two cubic MOFs based on redox-active catechol ligands [17,32,33]. In all these materials, charge is transported by a "through bond" pathway.

Besides the "through bond" pathway aforementioned, charge transport also occurs in a "through space" pathway (*i.e.*, $\pi\cdots\pi$ stacking interaction) [34–38]. For example, Yamashita *et al.* reported a porous semiconductor, the electrical conductivity in which is originated from the π-stacked columns of partially reduced NDI cores (NDI = 1,4,5,8,-naphthalenetetracarboxdiimide) [25]. Dincă *et al.* also reported a series of isostructural compounds M_2(TTFTB) (M = Zn, Co, Mn, Cd, and H_4TTFTB = tetrathiafulvalene tetrabenzoate). The TTF moieties in these compounds are associated through $\pi\cdots\pi$ interactions forming π-stacked columns which can act as charge transport channels [39]. These conductive π-stacked columns indicate the assembly of discrete molecules into supramolecular assemblies with π-stacked columns through $\pi\cdots\pi$ stacking interactions can be an alternative to the above-mentioned "through bond" strategy for constructing conductive frameworks. These supramolecular assemblies are promising to exploit new applications for their relatively better recyclability and solution-

* Corresponding authors.
E-mail addresses: lqh2382@fjirsm.ac.cn (Q.-H. Li), yghuang@fjirsm.ac.cn (Y.-G. Huang).

https://doi.org/10.1016/j.cclet.2022.108100
1001-8417/

processability compared to MOFs. Although some stable porous supramolecular frameworks based on intermolecular $\pi\cdots\pi$ stacking interactions have been reported [40–44], a cubic π-stacked framework structure with isotropic charge transport is still unknown. To enrich the library of isotropic conductive frameworks, the tripodal ligand L (L = tris(2-naphthimidazolylmethyl)amine) armed with three identical naphthimidazolmethyl moieties attract our attention. We envisage that molecules based on these ligands may self-assemble through $\pi\cdots\pi$ stacking interactions forming a cubic supramolecular framework with π-stacked columns in all three dimensions, thus leading to isotropic charge transport in the π-stacked structure.

In this work, we report a trinuclear $\{Ag^{I}_3\}$ compound $[Ag^{I}_3L_2]_2{\cdot}3OTf$ (**1**) which is characteristic of three pairs of π-stacked arms. The partially deprotonated cation self-assembles through hydrogen bonding and bidirectional $\pi\cdots\pi$ interactions giving rise to a chiral cubic srs framework with π-stacked helical columns along all of the three Cartesian coordinates, hence leading to isotropic charge transport.

The self-assembly of AgOTf with L in the mixture of MeOH, acetone, and DMF (8:3:1, v/v/v) gives rise to crystals of **1**. The IR spectrum and PXRD patterns for **1** are presented in Figs. S1 and S2 (Supporting information), respectively. **1** crystallizes in the cubic chiral space group $P4_132$ with the asymmetric unit containing one Ag^{I} ion, two independent one third of L ligands, and half of OTf^{-} anion. The existence of OTf^{-} in **1** is confirmed by X-ray photoelectron spectroscopy (XPS) study (Fig. S3 in Supporting information), and the abnormal conformation of OTf^{-} is due to the disorder induced by symmetry. A fan-shaped trinuclear $[Ag^{I}_3L_2]$ cation is formed in **1**. Considering half OTf^{-} exists in the asymmetric unit, the ligand must partially deprotonate to balance the negative charge from OTf^{-}. The $[Ag^{I}_3L_2]$ cation features three pairs of π-stacked arms (centroid-to-centroid distance of ~3.39 Å) (Fig. 1a). The $Ag^{I}\cdots Ag^{I}$ distance is ~2.99 Å in **1.**

In the crystal structure of **1**, each $[Ag^{I}_3L_2]$ associate with its three neighbors through intermolecular $\pi\cdots\pi$ interactions (centroid-to-centroid distance of ~3.59 Å) forming a chiral srs network with a Schläfli symbol of (10^3) (Figs. 1b and f) if treating $[Ag^{I}_3L_2]$ cations as nodes and the intermolecular $\pi\cdots\pi$ interactions as linkers (srs network represents the network of inorganic $SrSi_2$) [45]. Taking no account of the intermolecular $\pi\cdots\pi$ interactions, the same srs network also can be constructed by hydrogen bonding between $[Ag^{I}_3L_2]$ and OTf^{-} (Fig. 1c). Therefore, the srs network structure is enhanced by hydrogen bonding. The srs network can be described as an array of two types single-stranded helices. Each pair of π-stacked arms bidirectionally associate with two pairs from the neighboring $[Ag^{I}_3L_2]$ cations, giving rise to right-handed single stranded helical columns running along the three axes (Fig. 1d). These helical columns are generated around the crystallographic 4_1 screw axis, represent the first type of helix in the structure. Each π-stacked column serves as a second building unit and further associate with its four adjacent parallel neighbors leading to the chiral srs framework. Meanwhile, the second type of helix featuring large right-handed nanotube is generated (Fig. 1e). These two types of helices possess the same pitch length, but the shape and size are quite different because of the different components comprising the helical pitches. The helical pitch in the small helix is composed of a π-stack of four pairs π-stacked tris(2-naphthimidazolylmethyl) amine arms (Fig. 1d), while that in the large nanotube is composed of four groups of π-stacks consisting two pairs of π-stacked arms (Fig. 1e). OTf^{-} anions locate in the large right-handed nanotube hydrogen-bonding with the π-stack srs framework.

The UV-spectrum for the solution prepared by dissolving 1.0 mg **1** in 1.0 mL DMF shows a sharp absorption at ~266 nm and a broad absorption at ~328 nm, respectively (Fig. 2, down). These absorption bands may be attributed to the $\pi\rightarrow\pi^*$ and $n\rightarrow\pi^*$ transitions for L, respectively [46]. To give insight into the chirality of

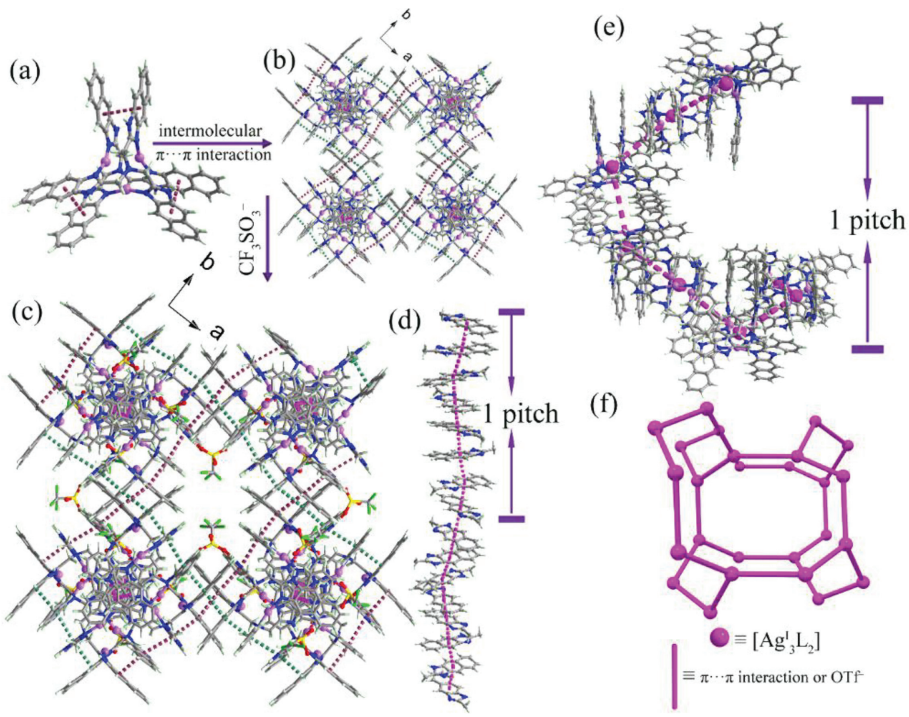

Fig. 1. (a) The trinuclear $[Ag^{I}_3L_2]$ cation in **1**. (b) The chiral π-stacked supramolecular structure constructed by intermolecular $\pi\cdots\pi$ interactions. The π-stacked helical columns along all of the three Cartesian coordinates are shown in dash line. (c) The framework structure of **1** built by OTf^{-} hydrogen bonding with $[Ag^{I}_3L_2]$. (d) The right-handed single stranded helical π-stacked column in **1**. (e) The large left-handed nanotube in **1** (The helix is shown in pink dash line). (f) Topology view of the chiral srs network of **1**.

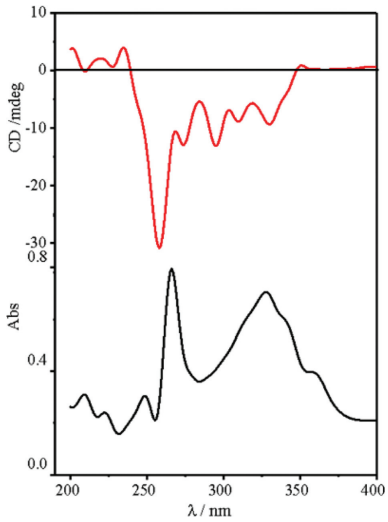

Fig. 2. The CD spectrum (up) and UV spectrum (down) for the solution of **1** in DMF.

1, CD measurement was also performed on the afore-mentioned solution. The result gives a negative Cotton effect for both the absorptions (Fig. 2, up), indicative of the chirality of $[Ag^{I}_{3}L_{2}]$ cations considering that the intermolecular hydrogen bonding and $\pi\cdots\pi$ interactions are disassociated in solution.

TG analysis for **1** under an argon stream demonstrates a weight loss of ~3.5% in the range of 30–120 °C, which can be attributed to the removal of solvent (Fig. S4 in Supporting information). However, the 3D π-stacked supramolecular structure collapses upon removal of solvent. **1** exhibits exceptional regeneration property. In specific, crystals of **1** can be readily recovered from the solution of **1** in mixed MeOH/acetone by recrystallization (Figs. S3 and S5 in Supporting information). Furthermore, **1** also shows great solution-processability. A thin film of **1** can be fabricated by a simple cast coating method (Figs. S3 and S6 in Supporting information). The great regeneration property and solution-processability enable **1** to be promising for further device-integration.

Since we successfully achieve π-stacked columns in all three dimensions in the cubic structure of **1**, the electric conductivity (σ) of the pellet of **1** is measured using the two-probe method at 300 K. The result gives a σ value of 2.01×10^{-7} S/cm, indicating the semi-conductivity of **1** (Fig. 3a). Compared with the reported conductive MOFs (Table S2 in Supporting information), the conductivity of **1** is not among the highest values. However, the σ value for **1** is remarkable for 3D isotropic conductive material and comparable to the porous cubic MOF based on catecholate reported by Dincă *et al.* [33]. To gain further insight into the semi-conductivity of **1**, UV–vis–NIR diffuse reflectance spectrum of powdered crystalline sample of **1** in the range of 200–2500 nm was recorded. **1** shows a broad strong absorption band in the range of

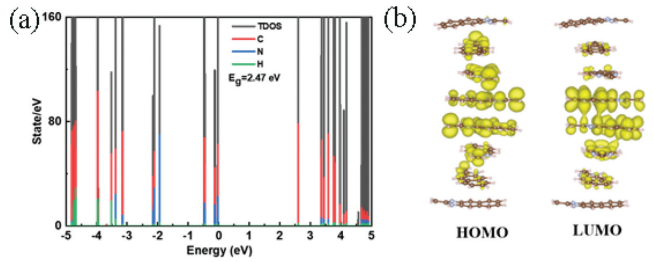

Fig. 4. (a) The calculated band gap for **1**. (b) The HOMO and LUMO distribution for **1**.

200–400 nm because of the $\pi \rightarrow \pi^*$ and $n \rightarrow \pi^*$ transitions for L. Extrapolating the linear part of the Absorption–Energy plot provides an approximate band gap of 2.33 eV indicative of the semi-conductivity of **1** (Fig. 3b). In addition, the IR, XPS, TGA, electrical conductivity, and UV–vis–NIR diffuse reflectance spectrum of re-generated **1** were also investigated (Figs. S1, S3, S4, S7 and S8 in Supporting information). All of the results are almost the same to those of **1** indicating the great recyclability of **1**.

To gain insight into the correlation between the semi-conductivity and the structure of **1**, DFT calculation using Vienna Ab-initio Software Package (VASP) [47,48] was performed to evaluate the band gap of **1**. The calculation was performed on a π-stacked column consisting of a helical pitch, because calculation on an infinite structure is impossible. The result gives a value of 2.47 eV slightly higher than the experimental result (Fig. 4a). From the HOMO and LUMO distributions of the helical column (Fig. 4b), it can be seen that the intermolecular $\pi\cdots\pi$ interactions are involved in the charge transport along the π-stacked column. Therefore, the intermolecular $\pi\cdots\pi$ interactions play an important role on the electrical conductivity of **1**.

In conclusion, a cubic chiral srs superstructure has been constructed by incorporation of hydrogen bonding and $\pi\cdots\pi$ interactions. The structure features π-stacked helical columns along all of the three Cartesian coordinates. The resulting supramolecular network structure provides a promising alternative to 3D isotropic MOFs where charges are expected to transport with equal efficiency along three dimensions. Besides the relatively high isotropic conductivity, this superstructure based on simple coordination cations also can be readily regenerated and shows great solution-processability. These features enable it to be potential for device integrations. Our findings open a new avenue toward processable isotropic conductive framework materials.

Declaration of competing interest

The authors declare that they have no known competing financial interests or personal relationships that could have appeared to influence the work reported in this paper.

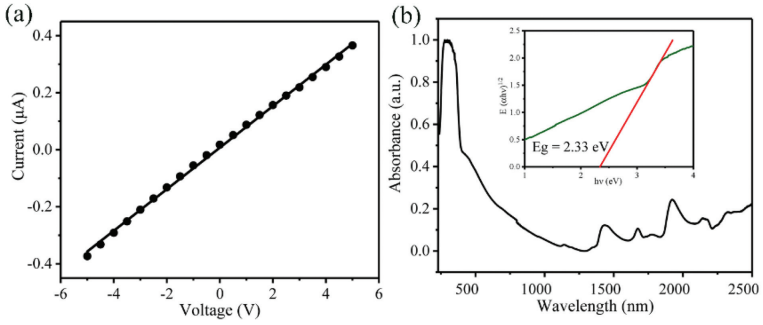

Fig. 3. (a) The *I–V* curve for **1** at room temperature. (b) The UV–vis–NIR diffuse reflectance spectrum of **1** (inset: the Tauc plot).

Acknowledgments

This work was supported by the National Natural Science Foundation of China (Nos. 21871262 and 21901242), the Natural Science Foundation of Fujian Province (No. 2020J05080), the Natural Science Foundation of Xiamen (No. 3502Z20206080), Fujian Science & Technology Innovation Laboratory for Optoelectronic Information of China (No. 2021ZR110), the Recruitment Program of Global Youth Experts, and Youth Innovation Promotion Association CAS (No. 2021302).

Supplementary materials

Supplementary material associated with this article can be found, in the online version, at doi:10.1016/j.cclet.2022.108100.

References

[1] M.L. Aubrey, M.T. Kapelewski, J.F. Melville, et al., J. Am. Chem. Soc. 141 (2019) 5005–5013.
[2] S. Zhang, X.B. Pei, W. Fan, J.Y. Xiong, J. Wang, Chin. Chem. Lett. 31 (2020) 1060–1070.
[3] I. Stassen, J.H. Dou, C. Hendon, M. Dincă, ACS Cent. Sci. 5 (2019) 1425–1431.
[4] L. Sun, M.G. Campbell, M. Dincă, Angew. Chem. Int. Ed. 55 (2016) 3566–3579.
[5] D.W. Feng, T. Lei, M.R. Lukatskaya, et al., Nat. Energy 3 (2018) 30–36.
[6] J.W. Liu, C.Y. Chen, K. Zhang, L. Zhang, Chin. Chem. Lett. 32 (2021) 649–659.
[7] K.W. Nam, S.S. Park, R. Reis, et al., Nat. Commun. 10 (2019) 4948.
[8] Z. Meng, A. Aykanat, K.A. Mirica, J. Am. Chem. Soc. 141 (2019) 2046–2053.
[9] D. Sheberla, J.C. Bachman, J.S. Elias, et al., Nat. Mater. 16 (2017) 220–224.
[10] X.J. Li, Q. Hu, H.P. Yang, et al., Chin. Chem. Lett. 33 (2022) 3657–3671.
[11] X.B. Liu, T. Yue, K. Qi, et al., Chin. Chem. Lett. 31 (2020) 2189–2201.
[12] S.S. Shinde, C.H. Lee, J.Y. Jung, et al., Energy Environ. Sci. 12 (2019) 727–738.
[13] X. Huang, P. Sheng, Z. Tu, et al., Nat. Commun. 6 (2015) 7408.
[14] A.A. Talin, A. Centrone, A.C. Ford, et al., Science 343 (2014) 66–69.
[15] T. Böttcher, I.K. Gal, R. Kolter, R. Losick, J. Clardy, J. Am. Chem. Soc. 135 (2013) 2927–2930.
[16] M. Hmadeh, Z. Lu, Z. Liu, et al., Chem. Mater. 24 (2012) 3511–3513.
[17] J.G. Park, M.L. Aubrey, J. Oktawiec, et al., J. Am. Chem. Soc. 140 (2018) 8526–8534.
[18] G. Skorupskii, B.A. Trump, T.W. Kasel, et al., Nat. Chem. 12 (2020) 131–136.
[19] X. Lin, E. Ning, X. Li, Q.W. Li, Chin. Chem. Lett. 31 (2020) 813–817.
[20] X.Y. Song, J.J. Liu, T. Zhang, L. Chen, Sci. China Chem. 63 (2020) 1391–1401.
[21] S.S. Park, E.R. Hontz, L. Sun, et al., J. Am. Chem. Soc. 137 (2015) 1774–1777.
[22] L.S. Xie, S.S. Park, M.J. Chmielewski, et al., Angew. Chem. Int. Ed. 59 (2020) 19623–19626.
[23] F. Solano, P. Auban-Senzier, L. Olejniczak, et al., Chem. Eur. J. (2022) e202203138.
[24] T.C. Narayan, T. Miyakai, S. Seki, M. Dincă, J. Am. Chem. Soc. 134 (2012) 12932–12935.
[25] L.Y. Qu, H. Iguchi, S. Takaishi, et al., J. Am. Chem. Soc. 141 (2019) 6802–6806.
[26] L.S. Xie, E.V. Alexandrov, G. Skorupskii, D.M. Proserpio, M. Dincă, Chem. Sci. 10 (2019) 8558–8565.
[27] Y. Lu, Y.Y. Zhang, C.Y. Yang, et al., Nat. Commun. 13 (2022) 7240.
[28] Y.B. Zou, T.X. Pan, Z.W. Fan, et al., Chem. Eng. J. 454 (2023) 140496.
[29] J.H. Dou, M.Q. Arguilla, Y. Luo, et al., Nat. Mater. 20 (2021) 222–228.
[30] M. Ko, L. Mendecki, K.A. Mirica, Chem. Commun. 54 (2018) 7873–7891.
[31] X.L. Deng, S.L. Zheng, Y.H. Zhong, et al., Coord. Chem. Rev. 450 (2022) 214235.
[32] F. Gándara, F.J. Uribe-Romo, D.K. Britt, et al., Chem. Eur. J. 18 (2012) 10595–10601.
[33] G. Skorupskii, M. Dincă, J. Am. Chem. Soc. 142 (2020) 6920–6924.
[34] J.Y. Koo, Y. Yakiyama, G.R. Lee, et al., J. Am. Chem. Soc. 138 (2016) 1776–1779.
[35] R. Reher, H.W. Kim, C. Zhang, et al., J. Am. Chem. Soc. 142 (2020) 4114–4120.
[36] J. Su, S. Yuan, J. Li, et al., Chem. Eur. J. 27 (2021) 622–627.
[37] X.Y. Wu, H.W. Wu, S.C. Wu, et al., Chem. Commun. 58 (2022) 2702–2705.
[38] Y. Yoshida, M. Maesato, Y. Kumagai, et al., Eur. J. Inorg. Chem. 24 (2014) 3871–3878.
[39] T.C. Narayan, T. Miyakai, S. Seki, M. Dincă, J. Am. Chem. Soc. 134 (2012) 12932–12934.
[40] J.H. Deng, J. Luo, Y.L. Mao, et al., Sci. Adv. 6 (2020) eaax9976.
[41] C. Chen, Z.Y. Di, H. Li, et al., CCS Chem. 4 (2022) 1315–1325.
[42] D. Meng, J.L. Yang, C. Xiao, et al., Proc. Natl. Acad. Sci. U. S. A. 117 (2020) 20397–20403.
[43] W.B. Wang, W. Zhai, Y. Chen, Q.Y. He, H. Zhang, Sci. China Chem. 65 (2022) 497–513.
[44] H.L. Zhu, H.Y. Chen, Y.X. Han, et al., J. Am. Chem. Soc. 144 (2022) 13319–13326.
[45] Y.G. Huang, B. Mu, P.M. Schoeneck, et al., Angew. Chem. Int. Ed. 50 (2011) 436–440.
[46] C. Davies, Fuel 52 (1973) 270–273.
[47] G. Kresse, J. Furthmuller, Comp. Mater. Sci 6 (1996) 15–50.
[48] G. Kresse, J. Furthmuller, Phys. Rev. B 54 (1996) 11169–11186.